



A compact readout platform for spectral-optical sensors

Roland Wuchrer¹, Sabrina Amrehn², Luhao Liu¹, Thorsten Wagner², and Thomas Härtling¹

¹Fraunhofer Institute for Ceramic Technologies and Systems IKTS, 01109 Dresden, Germany

²Department of Chemistry, University of Paderborn, 33098 Paderborn, Germany

Correspondence to: Roland Wuchrer (roland.wuchrer@ikts.fraunhofer.de)

Received: 21 February 2016 – Revised: 20 April 2016 – Accepted: 20 April 2016 – Published: 10 May 2016

Abstract. The continuous monitoring of industrial and environmental processes is becoming an increasingly important aspect with both economic and societal impact. So far, spectral-optical sensors with their outstanding properties in terms of sensitivity and reliability have not been considered as a potential solution because of the cost-intensive and bulky readout hardware. Here we present a card-size, inexpensive, and robust readout platform based on a wavelength-sensitive photodiode. In test and characterization experiments we achieved a wavelength shift resolution of better than 0.1 nm and a detection limit of 0.001 AU for ratiometric measurements. We furthermore discuss the capability and current limitations of our readout unit in context with interrogation experiments we performed with a photonic crystal-based fluid sensor. In sum we expect the presented readout platform to foster the exploitation of spectral-optical sensor technology for gas monitoring, chemical analytics, biosensing and many others fields.

1 Introduction

The development of spectral-optical sensors has advanced rapidly over the last decade, and some of these types of sensors are currently finding their way into industrial application. The two most promising working principles are the measurement of wavelength shifts of a single spectral peak and the ratiometric change of two-peak signals. Examples include localized surface plasmon resonance (LSPR) substrates (Steinke et al., 2015; Katzmann et al., 2012) and photonic crystal (PhC) structures (Amrehn et al., 2015) for biological and chemical sensing or gallium arsenide (GaAs) temperature fiber sensors (Willsch et al., 2014) and inorganic phosphor materials for thermometry (Klier and Kumke, 2015). Sensors made of these materials and structures are characterized by high sensitivity, electrical passivity, immunity against intensity fluctuations and applicability under extreme conditions (temperature, humidity, electromagnetic fields, etc.). However, their use is hampered by the available readout hardware.

The hardware providing the necessary spectral resolution (< 0.1 nm) typically lacks applicability for stable, easy-to-use and cost-efficient operation. Conventional interrogators such as grating spectrometers or interferometers pose difficulties

in terms of size and weight as they cannot be scaled down without loss of spectral resolution. Furthermore, they need highly demanding measuring conditions like vibration damping, air-conditioning and recalibration. Systems based on a tunable light source are restricted in their measurement range and are susceptible to environmental influences.

Consequently, for exploiting spectral-optical sensors in cost- and energy- efficient sensing systems, robust miniaturized high-resolution interrogation units are needed. One promising approach is photonic integrated circuit technology which exploits planar waveguide structures, e.g., arrayed waveguide gratings, to determine the wavelength information of an optical sensor signal. It is possible to produce small multifunctional chips with picometer resolution in a wafer process (see for example Evenblij and Leijtens, 2014). The major drawback of this technology is the restriction to single-mode waveguide structures. This implies that high-power light sources like superluminescence or laser diodes have to be used for an adequate signal-to-noise ratio, and the compatibility is limited to single-mode fiber sensors like fiber Bragg gratings or ring resonators. Otherwise the intensity loss in the light coupling elements is too high.

In the light of the approaches above, we believe that only with a holistic viewpoint on the entire sensor system

can a technically and economically successful sensor application be achieved. In particular, all components from the light source over the actual sensor to the interrogation unit need to be taken into consideration. In the same way, optoelectronic packaging technologies and reliability aspects have to be paid attention to in the design process. Following this credo, we present a compact photocurrent-based interrogation unit based on a wavelength-sensitive photodiode (WSPD) (Braasch et al., 1995; Lu et al., 1996). The key feature of the WSPD is a vertical stack of two photodiodes each having a different spectral sensitivity. This allows the determination of spectral changes in the irradiation light from the ratio of the two generated photocurrents. This approach combines the simplicity of an intensity measurement setup with the robustness of spectral readout and permits application of the interrogation unit for all kinds of spectral-optical sensors.

This article is structured as follows: in the first part we describe the working principle and the readout electronics of the WSPD. We then evaluate the performance of the setup for wavelength shift and ratiometric measurements and highlight advantages and difficulties. Finally, the capability of our readout unit is demonstrated with a photonic crystal-based fluid sensor.

2 Readout platform

The central element of the readout platform is the wavelength-sensitive photodiode WS7.56-TO5i (First Sensor AG). The WSPD is composed of two vertically stacked silicon photodiodes with different spectral response characteristics; see Fig. 1. Through this structure, the central wavelength of monochromatic signals or the centroid of a polychromatic light distribution can be determined by the ratio of the two generated photocurrents I_1 and I_2 . Therefore, it is ideally suited for the readout of spectral-optical sensors with their specific spectral changes. For reliable and high-resolution measurements, a low-noise electronics with a flexible amplification was realized. We chose a logarithmic amplifier (LOG112, Texas Instruments), which ensures a highly precise calculation of the current log ratio over a wide current input range of 7.5 decades (100 pA to 3.5 mA). The log ratio voltage V_{LOG} of the two photodiodes is computed by the LOG112 as follows:

$$V_{\text{LOG}} = 0.5 \text{ V} \cdot \log \frac{I_1(\lambda, P) + I_{\text{off1}}(T)}{I_2(\lambda, P) + I_{\text{off2}}(T)}, \quad (1)$$

where P describes the incident optical power and T the temperature of the photodiodes (formula adapted from the data sheet of the LOG112, Texas Instruments, 2005). The currents I_{off1} and I_{off2} denote offset values which allow considering that the temperature-dependence of the dark current and the noise behavior are different for the two stacked photodiodes. The noise effects of the amplifier electronics are also included. We would like to point out that intensity fluctuations

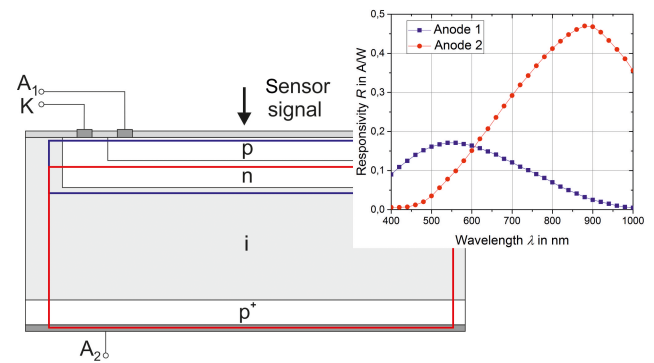


Figure 1. Photodiode structure and spectral responsivity curves of the WSPD (adapted from First Sensor WSPD data sheet, First Sensor AG, 2015).

tuations of the sensor signal have no influence on the readout because of the ratio calculation.

In most cases, a conversion of the calculated log ratio voltage into the centroid wavelength λ_C is not required for the readout of spectral-optical sensors, since the final calibration will be on the measured parameter, e.g., the refractive index. In general, the conversion will be carried out with a scale parameter s , which in the case of λ_C exhibits the unit nm V^{-1} :

$$\lambda_C = s \cdot V_{\text{LOG}}. \quad (2)$$

For many sensor applications, e.g., chemical analytics, a measurement rate in the range of several hertz is sufficient. So, to reduce the noise level of the calculated voltage signal, low-pass filtering with a cutoff frequency of 100 Hz was applied. Moreover, a stable power supply for a minimal noise level is crucial. Several voltage regulators were used to hold the necessary output voltages at a defined value regardless of the changes in the load current or input voltage.

As already mentioned, the dark current behavior of the stacked photodiodes of the WSPD is different. This results in a temperature dependent offset value for the log ratio voltage. For this reason, a temperature sensor (LM45B, Texas Instruments) was placed near the WSPD which enables a recalibration of the log ratio voltage.

In addition, an adjustable LED light source circuit was integrated into the electronics. It reflects the holistic approach we pursue in this work.

A 24 bit analog-to-digital converter, ADS1248 (Texas Instruments), resolves the measured data with high precision. Final processing and controlling of all signals are done with a microcontroller board (Arduino Uno), and the data are displayed with a LabVIEW program. The assembled circuit board is shown in Fig. 2.

A sub-miniature assembly (SMA) fiber adapter was implemented for both the WSPD and the LED, which ensures a stable and easy connection of multimode fibers for sensor irradiation and signal collection. The use of multimode fibers is possible as the WSPD operability is independent of

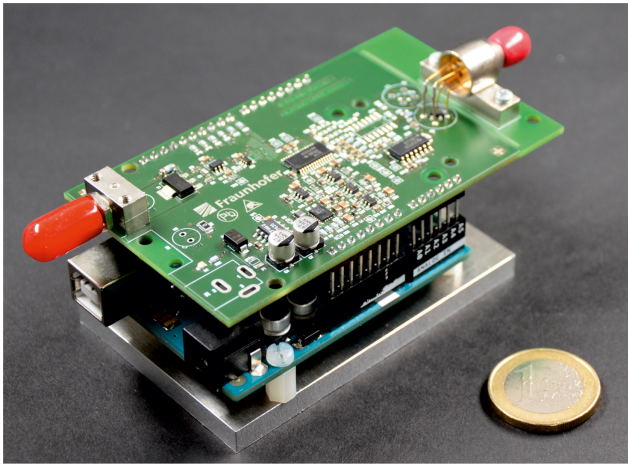


Figure 2. Photograph of the readout platform.

the angle of incidence, polarization, and the spatial intensity distribution of the light.

3 Test measurements

In a first evaluation experiment we tested the performance of the WSPD interrogation electronics for resolving peak wavelength changes and ratiometric response. The experiments were performed under laboratory conditions to guarantee a stable operating temperature for the WSPD. Furthermore, it was ensured that no interfering spectral peaks were present in the test signals and no stray light falsified the measurement. The focus of the test measurements was to characterize the resolution performance of the developed electronics, not the absolute wavelength accuracy.

A free space setup consisting of a white-light source (Xenon lamp) and different bandpass filters was used to determine the wavelength shift resolution. We used two bandpass filters with a central wavelength of 640 and 800 nm, respectively, and a full width at half maximum (FWHM) of 10 nm. By rotating the bandpass filters, their resonance condition was intentionally changed and the transmitted wavelength shifted to shorter wavelengths. The spectra at five rotation angles were analyzed for each filter with a high-resolution grating spectrometer (iHR550, Horiba) so as to obtain a spectral reference. The filtered light was alternately directed to the WSPD and the spectrometer by means of a multimode fiber. The light power at the fiber end was around $20 \mu\text{W}$. The acquired data are depicted in Fig. 3.

We observed a highly linear dependence between the centroid wavelength and the voltage ratio of the photodiodes. The measurement uncertainty was assumed as follows: the accuracy of the calibrated spectrometer is 0.07 nm, which represents the data point uncertainty of Fig. 3 in x direction. The temperature dependence of the WSPD output voltage was calculated out using the signal of the LM45B tem-

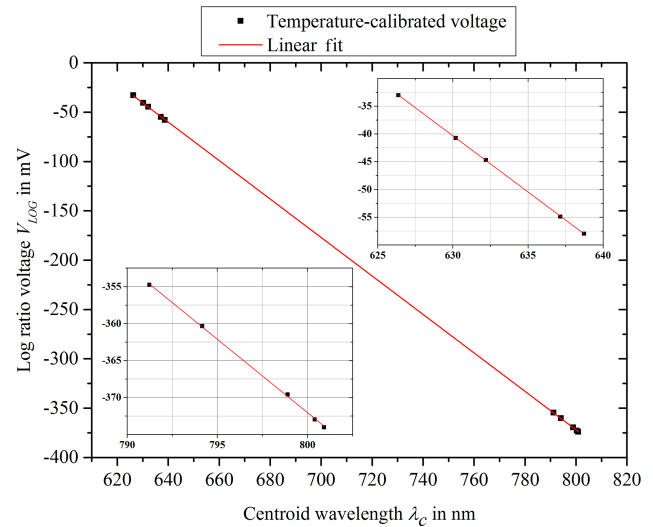


Figure 3. Measured log ratio voltage–centroid wavelength response of the readout platform.

perature sensor. From the data sheet of the latter we estimated a maximal error of 0.1 K for the temperature monitoring around room temperature (see data sheet of the LM45B, Texas Instruments, 2013). From separate experiments we determined the temperature dependence of the WSPD electronics to be approximately 1 mV K^{-1} , which in sum results in a systematical error of $100 \mu\text{V}$. To determine the statistical error of the interrogation electronics, the three-fold standard deviation was calculated from 1000 data points per measured wavelength. This represents a measurement time of 20 s. A maximal three-fold standard deviation of $30 \mu\text{V}$ and a corresponding standard error of $1 \mu\text{V}$ were obtained. For the linear fit of the 10 measured wavelengths a standard error of $1.2 \mu\text{V nm}^{-1}$ for the gradient was acquired. Hence, the resulting total error is $102 \mu\text{V}$ for the y direction of Fig. 3. In the face of these values we refrained from including error bars in the graphs in Fig. 1 since they could not be displayed clearly. In sum, a spectral shift accuracy of around 0.05 nm could be concluded for the WSPD interrogation electronics. The results and the linearly behavior are in agreement with experiments reported elsewhere (Amtor et al., 2011).

In our second experiment, we used two irradiation LEDs simultaneously to carry out a ratiometric measurement. For this, the light of the LEDs was coupled into a Y-type multimode fiber coupler and directed to the WSPD. A 525 nm LED, which was assembled on the circuit board, was varied in its forward current; i.e., its optical power was tuned. At the same time, a 624 nm LED was operated at constant current and worked as a baseline. This ensured that the measured peak ratio was independent of intensity fluctuations. A total light power in the range of 60 to $80 \mu\text{W}$ was measured at the end of the fiber coupler. As previously, reference spectra were recorded with the spectrometer to corre-

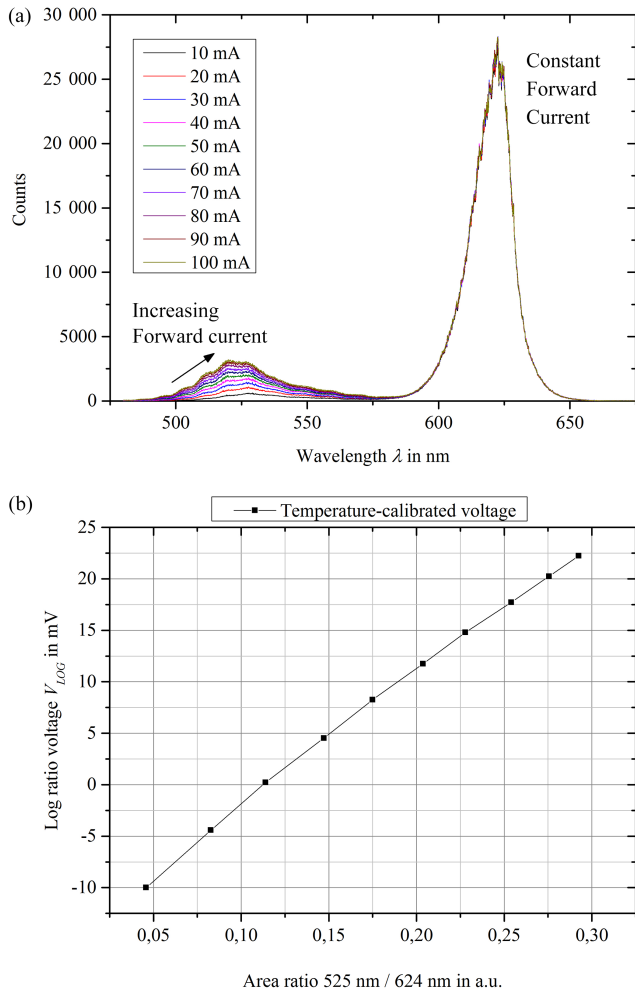


Figure 4. (a) Ratiometric spectra consisting of a baseline at 624 nm and a varying peak intensity at 525 nm. (b) Calculated ratios of the area under the respective emission curves to the measured log ratio voltage of the WSPD readout electronics.

late the LED emission ratio with the measured log ratio voltage. The emission spectra for different currents are depicted in Fig. 4a, while in Fig. 4b we plotted the ratio of the area under the emission curves of the respective LED over the output voltage ratio. In the latter diagram, a slight nonlinearity at small ratios is present, which is due to a nonlinear blueshift of the short-wavelength LED emission upon current tuning. This issue needs to be considered in real sensor applications in which the spectral positions of the peaks need be either constant or well known. As for the determination of the wavelength shift resolution, the temperature uncertainty with 0.1 K was the main error source. In the linear section of the diagram a resolution of LED emission ratio changes of 0.001 AU was achieved.

4 Demonstration of optical sensor interrogation

4.1 Photonic crystal-based fluid sensor

We chose to demonstrate the capability of the readout unit by interrogating a photonic crystal-based fluid sensor with the described electronics. PhCs are periodically ordered transparent nanostructures with a distinct boundary condition for the motion of photons through the crystal structure which result in unique optical material properties. The most well-known example of natural PhCs is probably opals which consist of periodically arranged silica spheres closely packed in 3-D. These gemstones generate iridescent colors (color changes depending on viewing angles). In analogy to the electronic band diagrams, which describe the allowed electronic states in a solid, the optical properties of the PhCs can be described in terms of photonic band structures. In this model the iridescent colors of opals are caused by the formation of photonic stop bands along different crystallographic directions. More details about PhCs can be found in textbooks, e.g., in Joannopoulos et al. (2008).

In the presented work artificially generated inverse opal structures made of tungsten oxide (WO_3) are utilized as sensing layers. They offer similar properties to the opals described above; in particular they exhibit photonic stop bands which can be observed in the reflection spectra (see Fig. 6). Amongst other things the position of the stop bands is very sensitive to the refractive index contrast of the inverse opal material and the material inside the pores, e.g., a fluid (Stein et al., 2008). Therefore a change of the refractive index of a fluid introduced into the pores can be monitored by determining the position of the reflection bands. In a previous work this was demonstrated utilizing a grating-based spectrometer as a readout device (Amrehn et al., 2015), which, however, is quite costly. As will be shown in the following, the diode-based readout unit presented here achieves comparable or even better performance without the need for additional data processing.

4.2 Experimental setup

Tungsten oxide inverse opals films were synthesized by a two-step casting process as follows: firstly, an artificial opal film consisting of poly(methyl methacrylate) (PMMA) spheres was deposited on a glass substrate by drop deposition. In the second step, the pores of the closely packed sphere arrangement were filled with a tungsten salt solution (99.99 % ammonium meta-tungstate hydrate, Sigma-Aldrich). After thermal conversion of the tungsten salt to tungsten oxide and combustion of the PMMA, the resulting tungsten oxide forms the ordered macroporous inverse opal framework. The spherical pores are positioned on the lattice points of the opal spheres. Further details of the synthesis are described elsewhere (Amrehn et al., 2015).

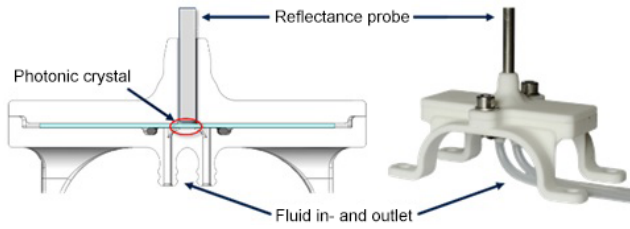


Figure 5. Scheme (left) and photo (right) of the custom-built fluid measurement cell.

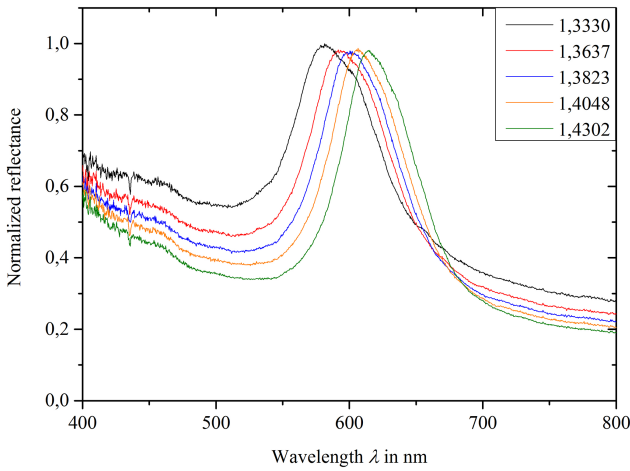


Figure 6. Normalized reflectance spectra of the WO_3 inverse opal structure infiltrated with different water-ethylene-glycol mixtures.

Utilizing a custom-built measurement cell (Fig. 5) and a reflection/backscattering probe (QR200-7-VIS-BX, Ocean Optics), the optical properties of the inverse opals were characterized. The samples were illuminated by a krypton light source (ecoVis, Ocean Optics) via the probe. Since the reflectance probe is mounted on the backside of the glass slide, it is not in contact with the sample media. The setup allows for continuous fluid measurements. When evaluating the optical properties of the sample, one has to keep in mind that the light has to pass through the glass slide and an additional interface (air/glass). The reflected light is collected by the reflectance probe and analyzed with the readout platform. Different mixtures of ethylene glycol and water were used for testing since this allows the refractive index to be varied over a relatively wide range. The refractive index of each mixture was determined with a refractometer (Krüss DR 201-95).

4.3 Results

Figure 6 shows the normalized reflectance spectra obtained with the described setup. In comparison to the narrowband signal (FWHM = 10 nm) used in the test measurements, the reflection spectra of the PhC structure have a FWHM of around 60 nm. In addition, the signal has an asymmetrical shape and a high baseline. It should be noted that, in con-

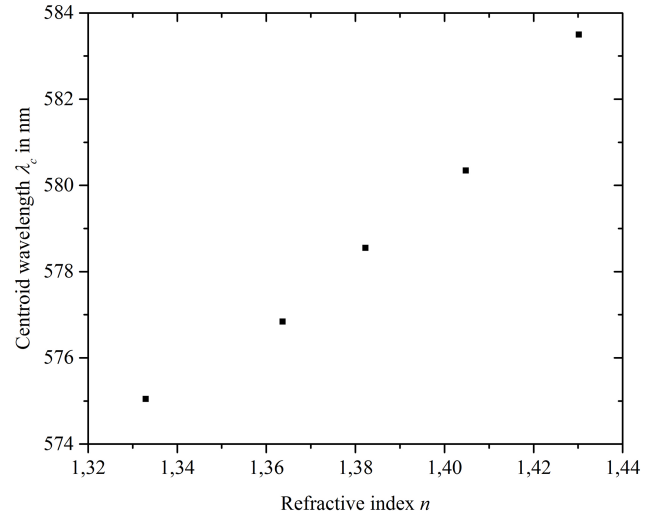


Figure 7. Centroid wavelength of the normalized reflection spectra from Fig. 6.

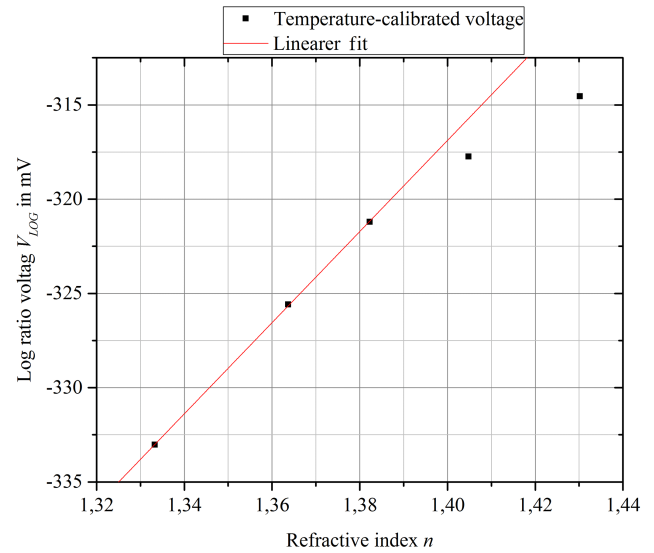


Figure 8. Measured voltages by the WSPD electronics for the PhC reflection spectra at different refractive indexes (Fig. 6).

trast to the measurements described in Sect. 3, the reflection spectra covered a very broad spectral window as depicted in Fig. 6. Figure 7 shows the centroids of the PhC spectra acquired with the grating spectrometer as reference data. A small nonlinearity of the wavelength shift can be seen. The data obtained with the WSPD readout electronics are illustrated in Fig. 8. From the linear part of the curve (lower refractive indexes) we estimate a limit of detection of 0.001 refractive index units. For higher refractive indices the curve deviates from the behavior of the reference data in Fig. 7. To further evaluate the WSPD data, we simulated the measured data as follows: the normalized reference spectra (Fig. 6) were multiplied with the two WSPD responsiv-

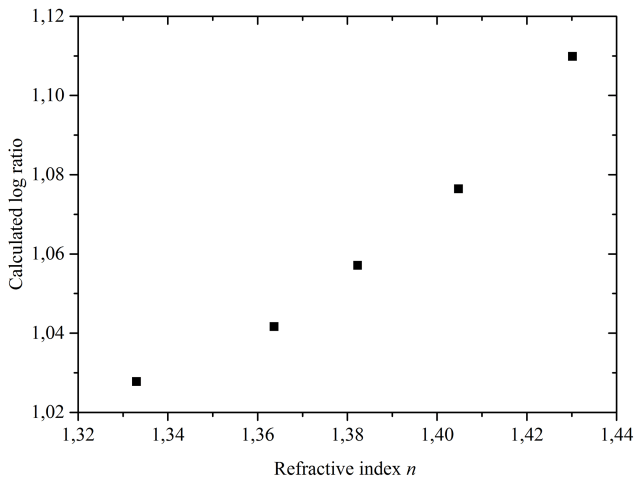


Figure 9. Calculated WSPD-measuring characteristics for the normalized reflection spectra from Fig. 6.

ity curves (Fig. 1). For the two sensitivity-folded spectra, the area under the curves was determined by summarizing the intensity values. Finally, the log ratio of these values was calculated. The result is displayed in Fig. 9. The calculated log ratio values for the WSPD are consistent in their behavior with the centroid wavelengths of the PhC reflection spectra in Fig. 7.

At the moment we cannot provide a satisfying explanation for the observed deviation. Several effects may lead to this behavior, which have to be investigated in depth in future work. These effects include the dependence of the refractive index sensitivity of the PhC on the wavelength, possible deviations of the WSPD element in use from the data sheet (especially at the edges of the broad spectral window), signal drift induced by an electronics artefact, and the higher signal-to-noise ratio induced by the low intensity in the PhC experiments (nW regime) in contrast to the test experiments (μ W range). Hence, further work will focus on the redesign of the PhC flow cell as well the WSPD readout electronics to improve the signal evaluation.

5 Conclusion and outlook

In this report we presented a compact electronics platform for reading out spectral-optical sensors and demonstrated its suitability for wavelength shift and ratiometric measurements. The system, based on a wavelength-sensitive photodiode, works independently of intensity fluctuations and permits a simple setup geometry similar to those used for common photodiodes. As the WSPD measures the centroid of the entire spectral distribution of the optical sensor signal, precise knowledge of the shape and spectral behavior of the signal is necessary in order to obtain optimal performance. Furthermore, the operating temperature of the WSPD has to be monitored or stabilized because of the different noise prop-

erties of the stacked photodiodes. In sum it can be concluded that for every sensor application an individual calibration of the WSPD electronic has to be done.

Finally, the applicability of the WSPD setup for the readout of a photonic crystal-based fluid sensor was shown. Although it was possible to unambiguously distinguish different refractive index media, these experiments also produced a slight mismatch between the measured signal and the reference data which is not yet understood. We will focus our future work on a deeper investigation of this observation. Moreover, a redesign of the entire electronics is planned, e.g., the integration of the microcontroller on the circuit board, to realize a compact system and reduce noise effects.

We summarize that, although the WSPD approach still has to overcome some challenges, the application-relevant characteristics like cost efficiency, miniaturization, high spectral resolution, robustness and simple handling are fulfilled with the setup we presented here.

Acknowledgements. The authors thank Hendrik Funke and Peter Blüthgen from Fraunhofer IKTS for remarks and work on the electronics. Also, the authors thank First Sensor AG, Berlin, for providing the responsivity data of the WS7.56. Furthermore, financial support from FhG Internal Programs (grant no. Attract 692271) and the German Federal Ministry of Education and Research (BMBF, grant no. 13N12969) is gratefully acknowledged.

Edited by: B. Jakoby

Reviewed by: two anonymous referees

References

- Amrehn, S., Wu, X., Schumacher, C., and Wagner, T.: Photonic crystal-based fluid sensors: Toward practical application, *Phys. Status Solidi A*, 212, 1266–1272, doi:10.1002/pssa.201431875, 2015.
- Amtor, T., Hofman, C. S., Knorz, J., and Weidemüller, M.: High-precision semiconductor wavelength sensor based on a double-layer photo diode, *Rev. Sci. Instrum.*, 82, 093111, doi:10.1063/1.3640409, 2011.
- Braasch, J. C., Holzapfel, W., and Neuschaefer-Rube, S.: Wavelength determination of semiconductor lasers: precise but inexpensive, *Opt. Eng.*, 34, 1417–1420, doi:10.1117/12.201655, 1995.
- Evenblij, R. S. and Leijtens, J. A. P.: Space Gator, a giant leap for fibre optic sensing, International Conference on Space Optics, Tenerife, Spain, 7–10 October, 2014.
- First Sensor AG: Wavelength-sensitive diode WS7.56-TO5i, available at: <http://www.first-sensor.com/en/products/optical-sensors/detectors/wavelength-sensitive-diodes-ws/index.html/> (last access: 19 February 2016), 2015.
- Joannopoulos, J. D., Johnson, S. G., Winn, J. N., and Meade, R. D.: *Photonic Crystals*, in: *Molding the Flow of Light*, 2nd Edn., edited by: Gnerlich, I., Princeton University Press, Princeton, 2008.

- Katzmann, J. and Härtling, T.: Nanorod formation by photochemical metal deposition in nanoporous aluminum oxide templates, *J. Phys. Chem. C*, 116, 23671–23675, doi:10.1021/jp303896a, 2012.
- Klier, D. T. and Kumke, M. U.: Upconversion NaYF₄:Yb:Er nanoparticles co-doped with Gd³⁺ and Nd³⁺ for thermometry on the nanoscale, *RSC Adv.*, 5, 67149–67156, doi:10.1039/C5RA11502G, 2015.
- Lu, G. N., Chouikha, M. B., Sou, G., and Sedjil, M.: Colour detection using a buried double p-n junction structure implemented in the CMOS process, *Electron. Lett.*, 32, 594–596, doi:10.1049/el:19960337, 1996.
- Stein, A., Li, F., and Denny, N. R.: Morphological Control in Colloidal Crystal Templating of Inverse Opals, Hierarchical Structures, and Shaped Particles, *Chem. Mater.*, 20, 649–666, doi:10.1021/cm702107n, 2008.
- Steinke, N., Wuchrer, R., and Härtling, T.: Aufbau und Biofunktionalisierung einer LSPR-Molekülsensoreinheit, 12th Dresden Sensor-Symposium, Dresden, Germany, 7–9 December 2015, 111–114, doi:10.5162/12dss2015/P2.2, 2015.
- Texas Instruments: Precision Logarithmic and Log Ratio Amplifiers LOG112/LOG2112, available at: <http://www.ti.com/general/docs/lit/getliterature.tsp?genericPartNumber=log112&fileType=pdf> (last access: 19 February 2016), 2005.
- Texas Instruments: LM45 SOT-23 Precision Centigrade Temperature Sensors, available at: <http://www.ti.com/general/docs/lit/getliterature.tsp?genericPartNumber=lm45&fileType=pdf> (last access: 19 February 2016), 2013.
- Willsch, M., Kaiser, J., Bosselmann, T., Wieduwilt, T., and Willsch, R.: Investigation of low-cost two-wavelength interrogation of different fiber optical temperature sensors into electric power facility monitoring systems, 23rd International Conference on Optical Fibre Sensors, Santander, Cantabria, Spain, 2–6 June 2014, 915796, doi:10.1117/12.2059269, 2014.